Journal of Nanobiotechnology

RESEARCH Open Access

Co-freezing localized CRISPR-Cas12a system enables rapid and sensitive nucleic acid analysis

Lifeng Zhang[1,4†], Shihua Luo[3,5†], Wenbin Li[1,2,7], Wanting Su[1,2], Siting Chen[1,2,7], Chunchen Liu[1,2], Weilun Pan[1,2], Bo Situ[1,2], Lei Zheng[1,2*], Ling Li[4,6*], Xiaohui Yan[1,2,7*] and Ye Zhang[1,2*]

Abstract

Rapid and sensitive nucleic acid detection is vital in disease diagnosis and therapeutic assessment. Herein, we propose a co-freezing localized CRISPR-Cas12a (CL-Cas12a) strategy for sensitive nucleic acid detection. The CL-Cas12a was obtained through a 15-minute co-freezing process, allowing the Cas12a/crRNA complex and hairpin reporter confined on the AuNPs surface with high load efficiency, for rapid sensing of nucleic acid with superior performance to other localized Cas12a strategies. This CL-Cas12a based platform could quantitatively detect targets down to 98 aM in 30 min with excellent specificity. Furthermore, the CL-Cas12a successful applied to detect human papillomavirus infection and human lung cancer-associated single-nucleotide mutations. We also achieved powerful signal amplification for imaging *Survivin* mRNA in living cells. These findings highlight the potential of CL-Cas12a as an effective tool for nucleic acid diagnostics and disease monitoring.

Introduction

Rapid and sensitive nucleic acid detection is vital for disease diagnosis, treatment monitoring, and pathogen detection [1]. Recently, emerging methods include electrochemical biosensors [2], surface-enhanced Raman spectra [3], and fluorescence platforms [4], of which the latter holds great potential for nucleic acid analysis due to its uniquely high sensitivity, ease of use, and capacity for real-time monitoring and in situ detection [5].

To develop a sensitive fluorescent platform for nucleic acid detection, multiple methods have employed signal tags comprised of nanomaterial tags and luminogens with aggregation-induced emission (AIEgens) [6, 7] or signal amplification strategies [8], such as rolling circle amplification [9], nucleic acid circuits [10], and CRISPR/Cas-based signal amplification [11]. In particular, CRISPR/Cas-based signal amplification has garnered much attention for its outstanding specificity and biocompatibility [12]. The CRISPR/Cas-based strategy relies on the utilization of CRISPR RNA (crRNA) binding to a specific target DNA or RNA sequence [13]. With the aid of Cas proteins, this crRNA-target complex enables the precise identification and digestion of nucleic acids [14]. Although CRISPR/Cas-based strategies are widely applied, they are not sensitive enough to serve as an ideal nucleic acid testing method. To address this limitation,

†Lifeng Zhang and Shihua Luo contributed equally to this work.

*Correspondence:
Lei Zheng
nfyyzhenglei@smu.edu.cn
Ling Li
liling@smu.edu.cn
Xiaohui Yan
gzyanxh@126.com
Ye Zhang
zhangye232@i.smu.edu.cn

Full list of author information is available at the end of the article

Graphical abstract

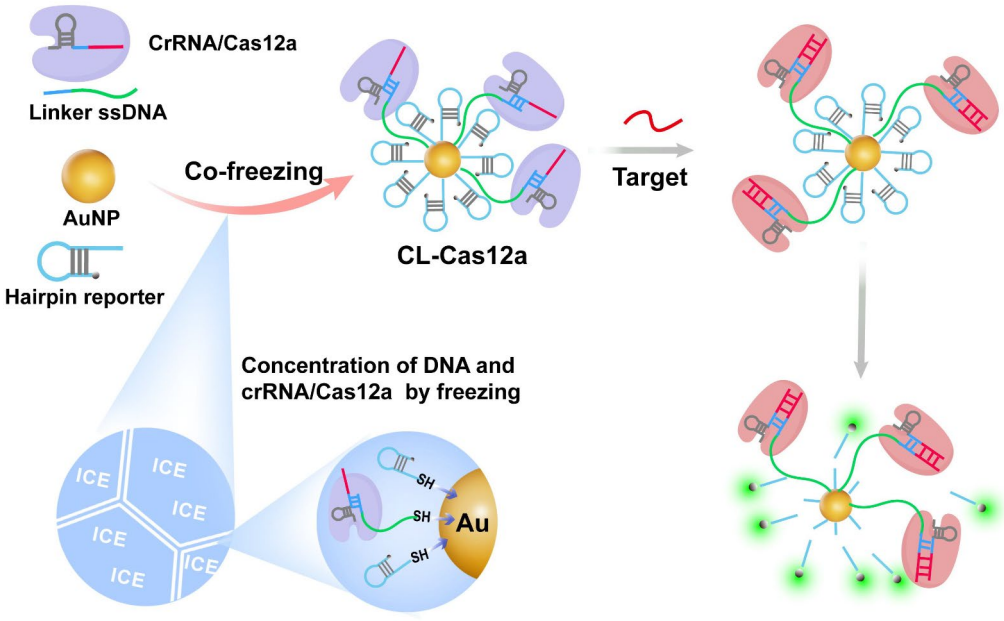

Keywords CRISPR-Cas12a, Localized reaction, Co-freezing, Nucleic acid analysis

nucleic acid amplification is employed to augment the target abundance before detection, thereby enhancing the sensitivity of CRISPR/Cas-based molecular diagnostics [15]. However, it extends the detection time and introduces potential limitations for subsequent analysis, including false-positive signals [16, 17] and cross-interference [18]. Furthermore, the two-step reaction system significantly escalates the risk of aerosol contamination, posing challenges in accuracy and safety [19]. These considerations highlight the need for alternative approaches that can circumvent these limitations and streamline the detection process in a more efficient and reliable manner.

In order to improve the amplification efficiency of CRISPR/Cas system without background signal leakage, the strategy of surface confinement is proposed. For example, Yang et al. used DNA tetrahedron to load reporters to form framework reporters, which enables sensitive and rapid detection of pathogen nucleic acids [20]. However, limited load sites of DNA tetrahedron restricted the further amplification of CRISPR/Cas system. Luo et al. established AuNPs reporter, which is more sensitive than that of the ssDNA reporter system [21]. Nonetheless, prefabrication of AuNPs reporter and Cas12a system is time-consuming and complicated. Therefore, it is very necessary to construct a high density localized CRISPR-Cas system with simple preparation.

DNA-functionalized Au nanoparticles is important for assembly, biosensing, and therapeutics, featuring dense arrays for better stability and cellular uptake [22–24]. DNA-functionalized Au nanoparticles are traditionally made using gold-thiol bonds, but early methods were slow, requiring two days of stepwise salt addition [25]. To simplify this, Liu et al. introduced a quicker method using low pH for DNA attachment, but it needs an extra acidic buffer to neutralize the solution after labeling, making the process complex [26]. Deng et al. reported an efficient method using evaporation, but it it requires a rotary evaporator and additional reagents, which increases the complexity of the operation [27]. Recently, a reagent-free labeling method was developed, which attaches DNA probes to the surface of AuNPs using a freeze-based approach [28, 29]. During the freezing process, nucleic acids concentrate in the gaps between ice crystals, leading to the assembly of nucleic acids onto AuNPs and the process is very simple, fast, and efficient [30].

Herein, a sensitive and simple fluorescence platform based the co-freezing localized CRISPR-Cas12a (CL-Cas12a) was developed for nucleic acid analysis in this study. The CL-Cas12a system was synthesized via a simple co-freezing method, in which AuNP, linker ssDNA, hairpin reporter, and Cas12a/crRNA complex were concentrated in the voids between ice microcrystals, resulting in rapid and high-efficiency assembly (Scheme 1A). Benefit from the CL-Cas12a, this biosensor demonstrated a high sensitivity and specificity for nucleic acid detection. Moreover, the proposed platform

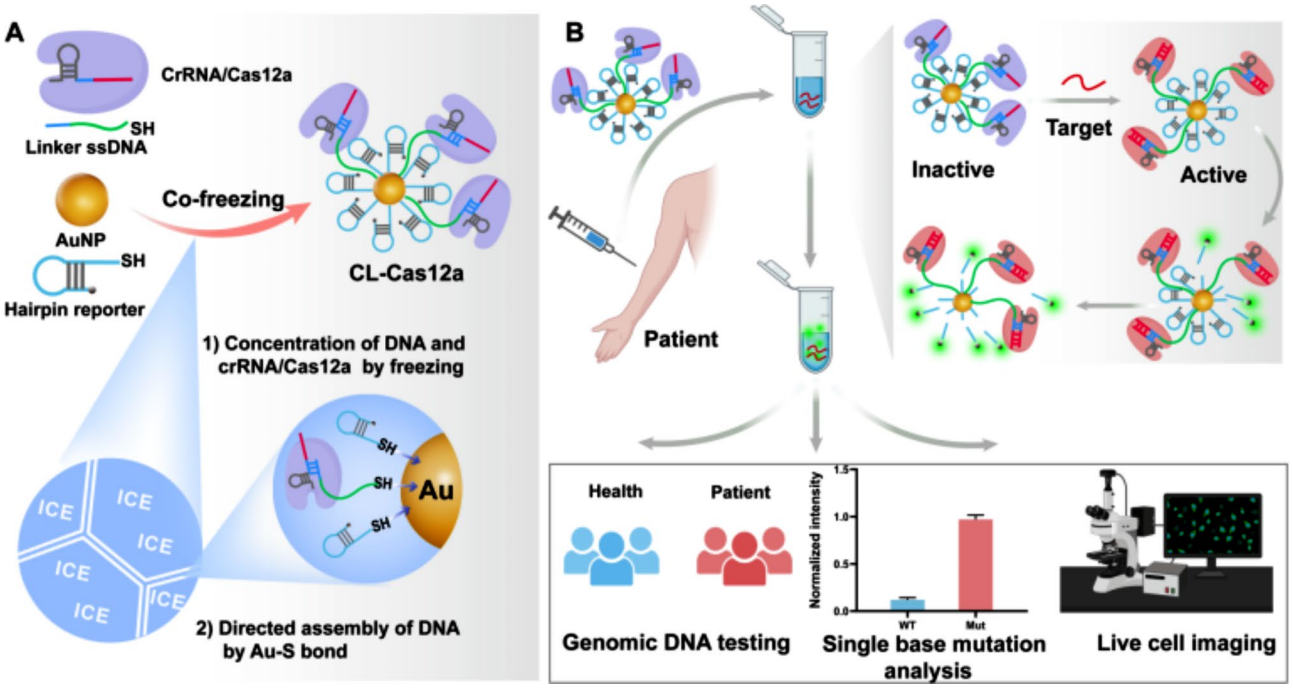

Scheme 1 Schematic illustration of the CL-Cas12a platform. (**A**) Construction of the CL-Cas12a using the co-freezing method. This process involves concentrating the hairpin DNA and crRNA/Cas12a complex into the voids between ice microcrystals, subsequently, the hairpin DNA and crRNA/Cas12a complex assemble directly through Au-S bonds. (**B**) The CL-Cas12a platform applied for biological applications, including DNA testing, single-base mutation analysis, and live cell imaging

was successful adopted for DNA testing and single-base mutation analysis in clinical samples. Additionally, we also applied CL-Cas12a system for imaging intracellular *Survivin* mRNA (Scheme 1B). Compared other L-Cas12a systems, this CL-Cas12a offers several advantages. Firstly, it eliminates the requirement for tedious preparation and preamplification, significantly reducing processing time. Secondly, CL-Cas12a with high load efficiency greatly enhances local concentrations of crRNA/Cas12a complex and its substrate hairpin reporter, which serves as a programmed track. Once the driving motor, crRNA/Cas12a, is triggered by targets, the CRISPR-Cas12a system moves along the surface of the AuNPs, generating a cascade of signal outputs. Thirdly, because of CL-Cas12a's high DNA density to improve nuclease degradation resistance, it is extremely stable and has a low background in biological samples, allowing for increased sensitivity in clinical applications and in situ living cells imaging.

Results

Characterization of the CL-Cas12a system

The assembly of the CL-Cas12a system was validated using transmission electron microscopy (TEM). In contrast to the round structure and dispersed nature of AuNP (Fig. 1A), CL-Cas12a produced a distinct 3-nm protein layer, indicating successful modification of AuNPs with the Cas12a/crRNA complex (Fig. 1B). Size distribution analysis by DLS (Dynamic Light Scattering) showed approximate sizes of 25 nm (AuNP), 28 nm (DNA-AuNP), and 32 nm (CL-Cas12a) (Fig. 1C), consistent with the TEM findings. The zeta potential of AuNPs was −5.65 mV. After DNA loading, the zeta potential of DNA-AuNP shifted to −12.19 mV, indicating an increase in charge. In contrast, the CL-Cas12a system had a zeta potential of −1.47 mV due to the positively charged Cas12a (Fig. 1D). CL-Cas12a (529 nm) also showed a 9-nm UV-vis redshift compared to AuNP (520 nm) and a 7-nm redshift of DNA-AuNP (522 nm) (Fig. 1E). To verify the feasibility, the trans-cleavage ability of Cas12a for hairpin reporter was confirmed by PAGE (Polyacrylamide Gel Electrophoresis) analysis (Figure S1). When the target is present, producing obvious fluorescence, and negligible fluorescence when there is no target (Fig. 1F). And the freezing did not affect the performance of CL-Cas12a (Figure S2). These results demonstrating the successful assembly and the feasibility of the proposed CL-Cas12a system.

The superior performance of CL-Cas12a

To confirm the superior performance of CL-Cas12a, three modes were used: (a) typical Cas12a system; (b) salt-aging for building the localized Cas12a (L-Cas12a). (c) Co-freezing of hairpin reporter and crRNA/Cas12a complex to construct the CL-Cas12a (Fig. 2A). CL-Cas12a yielded the highest fluorescence response (F/F_0) and reached saturated fluorescence within just 35 min,

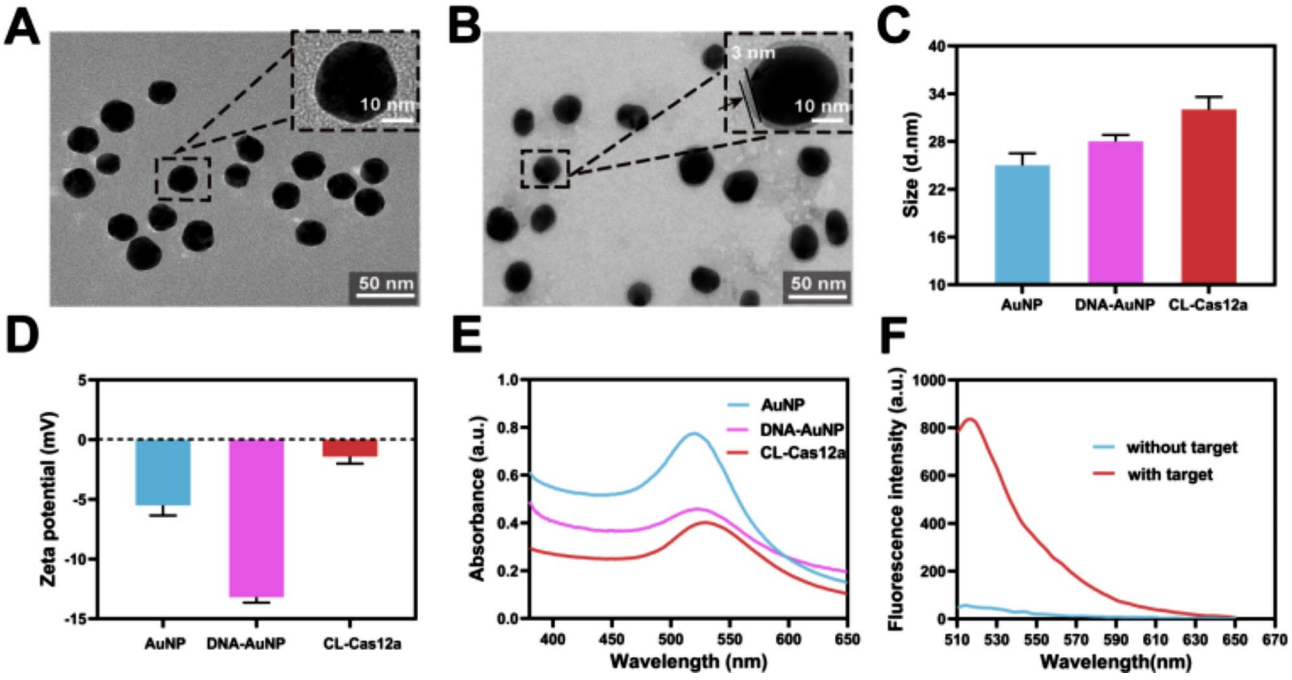

Fig. 1 Characterization of the CL-Cas12a system. TEM image of (**A**) AuNP and (**B**) CL-Cas12a (scale bars: 50 nm; scale bar in magnified image: 10 nm). (**C**, **D**, **E**) DLS analysis, Zeta potential, and UV-vis absorbance spectra of AuNP, DNA-AuNP and CL-Cas12a. (**F**) Fluorescence spectrum of constructed CL-Cas12a system without target and with target. Error bars represent standard deviations of the measurements ($n = 3$)

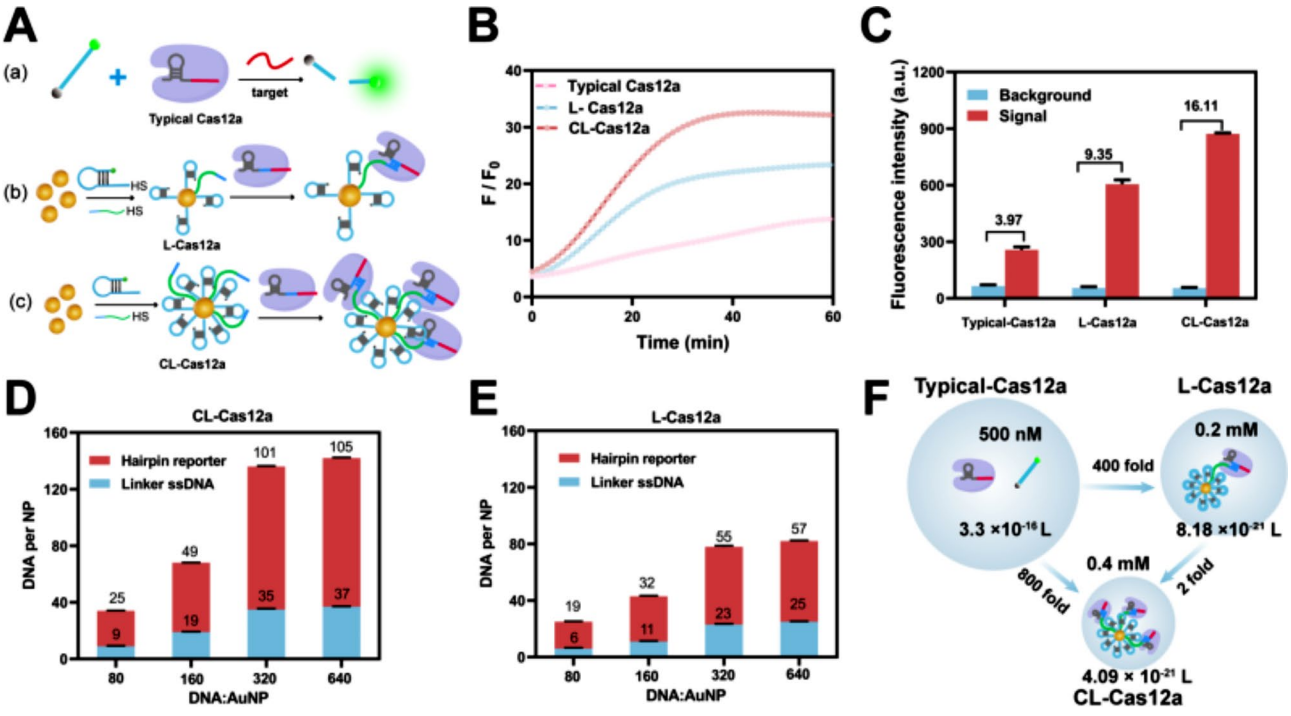

Fig. 2 (**A**) Schematic diagram of three types of CRISPR-Cas12a based systems. (**B**) Real-time fluorescence graphs corresponding to three kinds of CRISPR-Cas12a based system. (**C**) Signal-to-noise ratio of the three kinds of probes. The number of hairpin reporter and linker ssDNA bound to AuNPs in CL-Cas12a (**D**) and L-Cas12a (**E**). (**F**) Comparison of the reaction space and local concentration of typical-Cas12a, L-Cas12a, and CL-Cas12a

while the L-Cas12a and typical Cas12a required 45 min and 1 h, respectively (Fig. 2B). Fluorescence measurements for the different Cas12a systems were 257.0 (Typical-Cas12a), 605.0 (L-Cas12a), and 872.0 a.u. (CL-Cas12a), with corresponding background signals of 64.6, 54.0, and 54.0 a.u, respectively. CL-Cas12a produced the highest signal-to-background ratio (16.11 S/B) (Fig. 2C), ensuring robust sensitivity and specificity. Without the addition of linker DNA, the Cas12a demonstrated a slower reaction rate and a lower signal-to-noise ratio compared to CL-Cas12a (Figure S3). These results showed that CL-Cas12a exhibits significantly greater activity due to the increased local concentration of substrates achieved through spatial confinement. Interestingly, CL-Cas12a obtain the maximum load efficiency at the ratio of DNA: AuNP of 320 (Fig. 2D), which is about twice more than that L-Cas12a using the method of salt aging (Fig. 2E). Compare with CL-Cas12a constructed, the stepwise freezing Cas12a (SL-Cas12a) have greatly higher ratio between hairpin reporters and linker ssDNA and relative low fluorescent signal (Figure S4). This may occur as a result of the hairpin reporters occupying the locations, preventing the linker ssDNA from binding to the AuNP during stepwise freezing, leading to a deterioration in trans-cleavage efficiency of Cas12a.

The enhanced sensitivity of the CL-Cas12a system was further validated using the principles of collision theory, characterized by the equation V=1/cN. Here, 'N' denotes the Avogadro constant, 'C' signifies the concentration of reactants, and 'V' represents the volume of the local sphere. Following the conjugation of Cas12a and the reporter to AuNPs to form L-Cas12a, the spatial proximity between Cas12a/crRNA and the reporter was significantly reduced to 25 nm. This proximity modification led to a notable increase in the local concentrations of Cas12a/crRNA and reporter, reaching up to 0.2 mM. In the context of the CL-Cas12a system, the concentration of Cas12a/crRNA and reporter on the AuNPs nearly doubled, further elevating the local concentration to approximately 0.4 mM. A direct correlation was observed between the frequency of collisions and the concentration of the hairpin, indicating that the accelerated reaction kinetics in the CL-Cas12a system can be attributed primarily to the increased local concentration (Fig. 2F).

Analytical performance of proposed platform

Before demonstrating the analytical performance of this biosensor, we first optimized several reaction parameters, including incubation time (30 min) and temperature (37 ℃) (Figure S5). To achieve better performance of CL-Cas12a, the number of linker DNA connect to crRNA and ratio of the linker DNA to hairpins were optimized as 10 bp and 1:3, respectively (Figure S6 and S7). To demonstrate the superior sensitivity of the CL-Cas12a system, we conducted fluorescence analysis on CL-Cas12a (Fig. 3A), L-Cas12a (Fig. 3D), and typical Cas12a (Figure S8) using different concentrations of target HPV16. As shown in Fig. 3B, the fluorescence intensity (FI) significantly increased with increasing target concentration. The CL-Cas12a based biosensor exhibited a broad linear detection range from 100 aM to 1 pM, with a correlation of FI=37.5136 $\lg C_{target}$ + 210.9398 (R^2=0.994) (Fig. 3C). Using the blank+3SD rule, the limit of detection of the CL-Cas12a was found to be as low as 98 aM, which is 969-fold lower than that of L-Cas12a (Fig. 3E and F) and 9138-fold lower than that of typical Cas12a (Figure S8), demonstrating the superior sensitivity of the proposed CL-Cas12a system.

In addition to high sensitivity, having high specificity is extremely important in molecular diagnostics. The specificity of this platform was assessed by detecting five HPV subtypes (HPV 06, 18, 31, 33, and 58). The FI from the target DNA was 7 times higher than that of other analogous sequences as shown in Fig. 3G, highlighting the high selectivity of the CL-Cas12a. Besides, we also evaluate the specificity of CL-Cas12a by testing its ability to discriminate against SM. A series of targets containing SM were analyzed by CL-Cas12a. The system shown excellent recognition of mutations at the proximal (3 ') end of the target (Fig. 3H). However, when mismatches are in the middle of the spacer sequence (SM8-SM14), its recognition ability decreased significantly (Figure S9A). For mutations at the other end of the spacer sequence (SM15-SM23), it almost lacks the capability to recognize base mutations (Figure S9B). Reproducibility testing of CL-Cas12a against 1 pM and 100 pM samples (Figure S10) showed intra- and interbatch coefficients of variation of 2.50–4.32%, demonstrating the excellent reproducibility of this CL-Cas12a. Additionally, the color of the CL-Cas12a system remains pink and is unchanged after being stored for 25 days at 4 °C. The fluorescence signal also remains essentially constant within the first 15 days, demonstrating that the system has good stability (Figure S11). In general, compared to other L-Cas12a system for detecting nucleic acid (Table S1), the developed platform based CL-Cas12a is more simple-to-prepared and sensitive.

Analysis of the DNA from infected cells

Accurate detection of human papillomavirus (HPV) is essential for clinical treatment of HPV-related cervical cancer and genital warts [31]. We used a model of HPV16-infected cultured cervical cancer cells (CaSki) and directly analyzed the total extracted DNA with the CL-Cas12a system (Fig. 4A). As illustrated in Fig. 4B, CL-Cas12a differentiated HPV16-infected cells from uninfected controls, including HPV18-infected HeLa cells and 16HBE cells, consistent with previous findings [32].

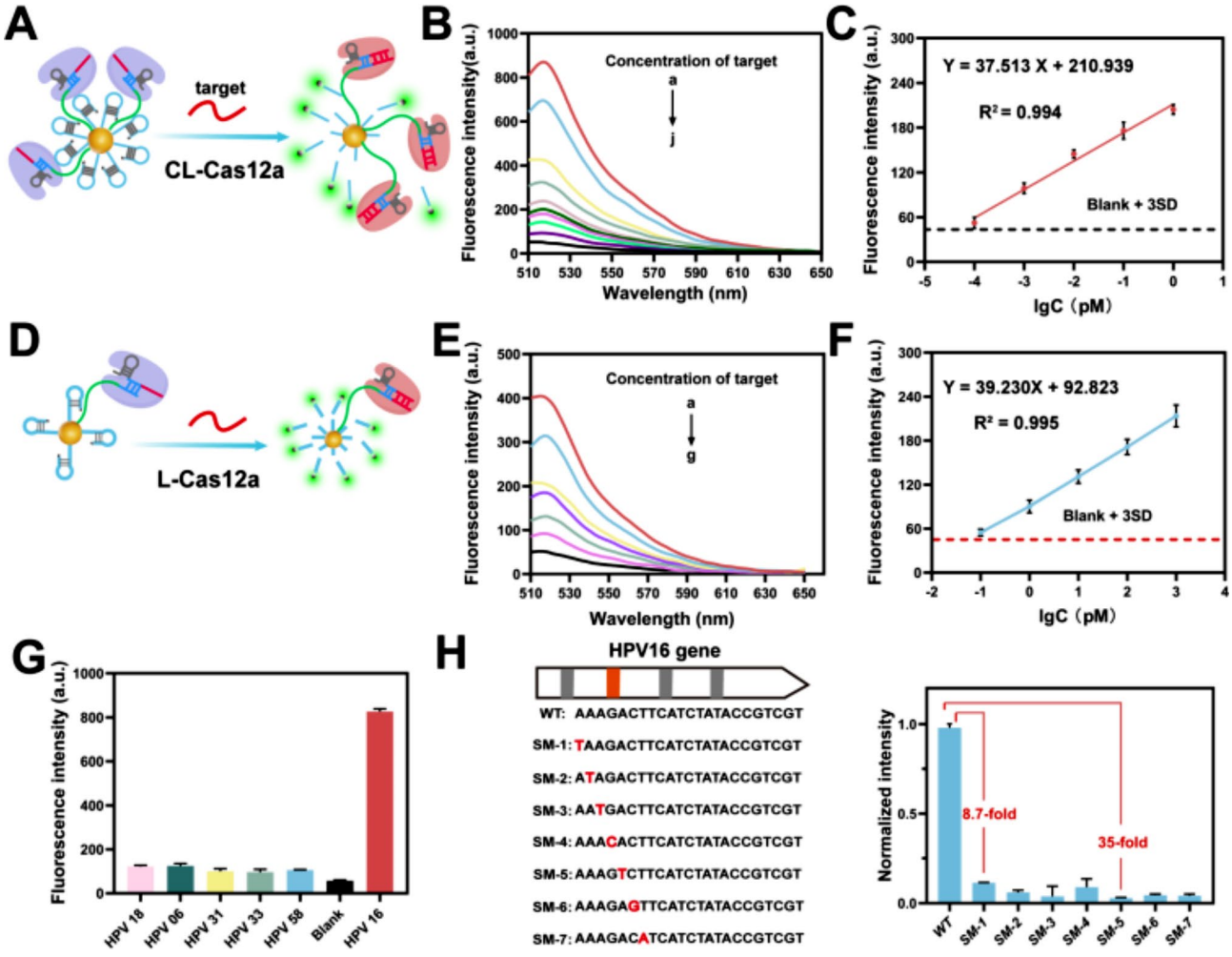

Fig. 3 (**A**) Schematic diagram of CL-Cas12a based systems. (**B**) Analytical performance of the CL-Cas12a strategy in vitro. Fluorescence intensity curve with the target concentration from a to j (100 nM, 10 nM, 1 nM, 100 pM, 10 pM, 1 pM and 100 fM, 10 fM, 1fM, and 100 aM). (**C**) Corresponding calibration of target HPV16 in CL-Cas12a strategy. (**D**) Schematic diagram of L-Cas12a based systems. (**E**) Analytical performance of the L-Cas12a strategy in vitro. Fluorescence intensity curve with the target concentration from a to g (100 nM, 10 nM, 1 nM, 100 pM, 10 pM, 1 pM and 100 fM). (**F**) Corresponding calibration of target HPV16 in L-Cas12a strategy. (**G**) Fluorescence intensity respond to the target HPV 16, five HPV subtypes, and blank with a concentration of 100 nM. (**H**) Sequence information and the normalized fluorescence signals of the wild-type (WT) target and SM strands. The mutation site is indicated in red

We also used CL-Cas12a to quantify target DNA and confirmed the results by PCR. CL-Cas12a could detect as few as 500 copies/μL of HPV DNA from infected cells. In contrast, the typical Cas12a system required 5×10^6 copies/μL of HPV DNA to generate detectable signals, underscoring the remarkable sensitivity of CL-Cas12a (Fig. 4C).

To assess the practical utility of CL-Cas12a for clinical diagnosis, we analyzed crude DNA extracted from cervical swabs obtained from 7 healthy donors and 13 patients with HPV16 virus infection (Fig. 4D; Table S3). CL-Cas12a identified HPV DNA in patient serum samples, distinguishing them from samples obtained from healthy donors (Fig. 4E), and the fluorescence signals produced by CL-Cas12a correlated with the quantitative real-time PCR results (Fig. 4F and S12). We thus established the ability of CL-Cas12a to directly and accurately detect HPV infection in clinical samples with exceptional sensitivity and precision.

Analysis of cancer-related single-base mutation

Single-base mutation is one of the most common mutation types in the human genome. It is closely related to phenotypic changes [33], gene function [34], human characteristics [35], and disease occurrence [36]. Current technologies for detecting single-base mutations, such as ddPCR, NGS, and Sanger sequencing, have their limitations. ddPCR [37] is expensive and limited in sample throughput; NGS [38] requires significant cost and complex data processing; Sanger sequencing [39] has low sensitivity and throughput. Therefore, it is important to

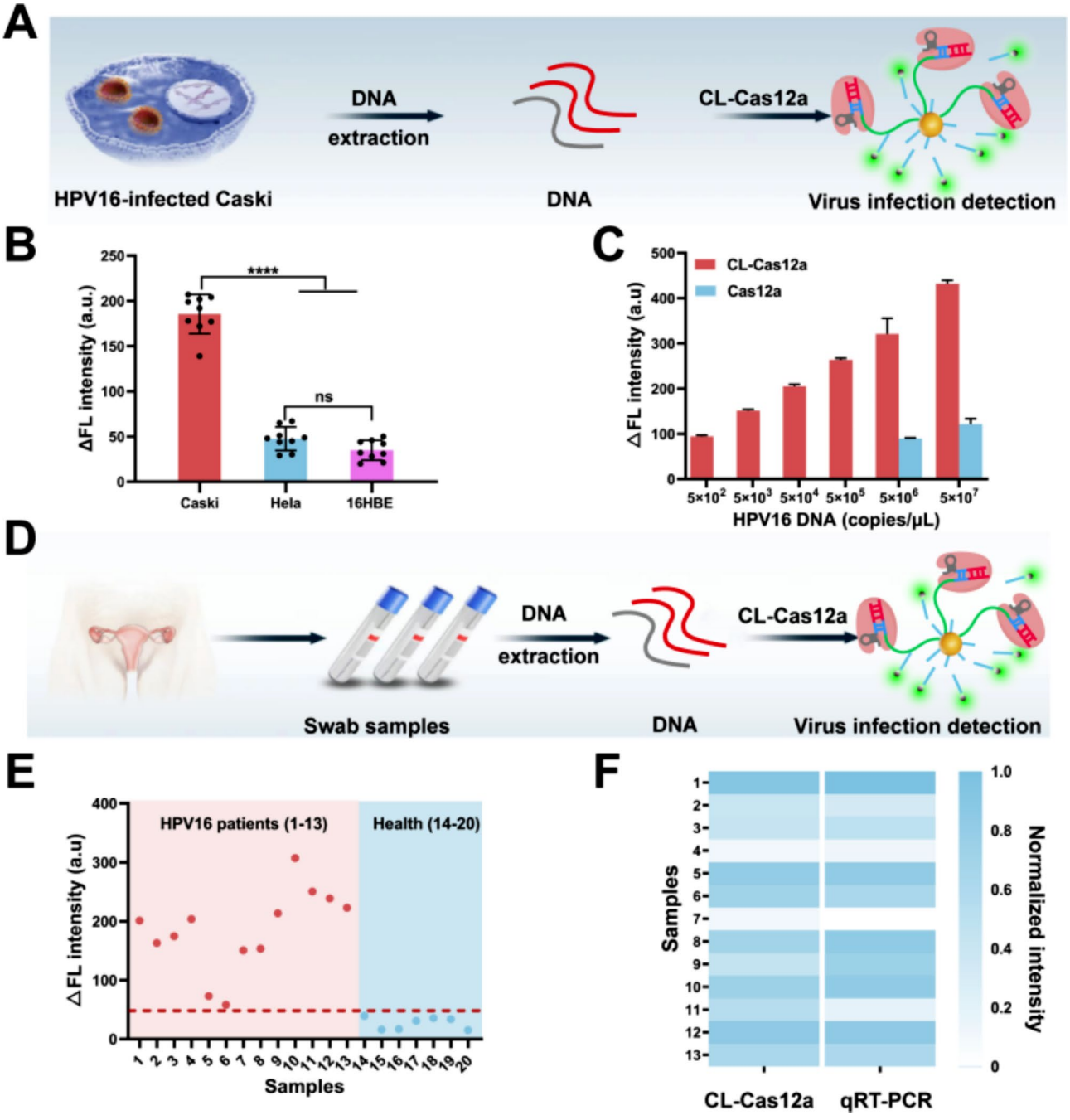

Fig. 4 Evaluation of CL-Cas12a for virus infection diagnosis. (**A**) Schematic illustration for the analysis of HPV infection in cultured cervical cancer cells (CaSki and HeLa) by CL-Cas12a. (**B**) Fluorescence signals of HPV16 infected cells CaSki and HPV18 infected cells HeLa and human bronchial epithelial cells 16HBE samples. (**C**) Fluorescence signals of different amounts of DNA from HPV16-infected CaSki in CL-Cas12a and the typical L-Cas12a. (**D**) Schematic of HPV infection detection in human cervical swab samples by CL-Cas12a. (**E**) The fluorescence signals of 20 serum samples in CL-Cas12a. Cervical swab samples from thirteen patients (1 to 13) with HPV virus infection and seven healthy donors (14 to 20) were tested, respectively. (The red dash line indicates cut off value). (**F**) Heatmap of the normalized signal intensities of thirteen patient samples in CL-Cas12a and qRT-PCR. Data represent means ± SD. **** $p < 0.0001$)

develop a simple and efficient method to detect single-base mutations.

The high specificity of CL-Cas12a promote us to distinguish cancer-related single-base mutations in clinical samples. We evaluated the performance of CL-Cas12a by targeting the KRAS_34G > T mutation, which common in various cancers, especially in non-small cell lung cancer [40, 41] (Fig. 5A). DNA extracted from lung cancer tissues was analyzed and confirmed through histopathology and DNA sequencing. The origin of these tissues had

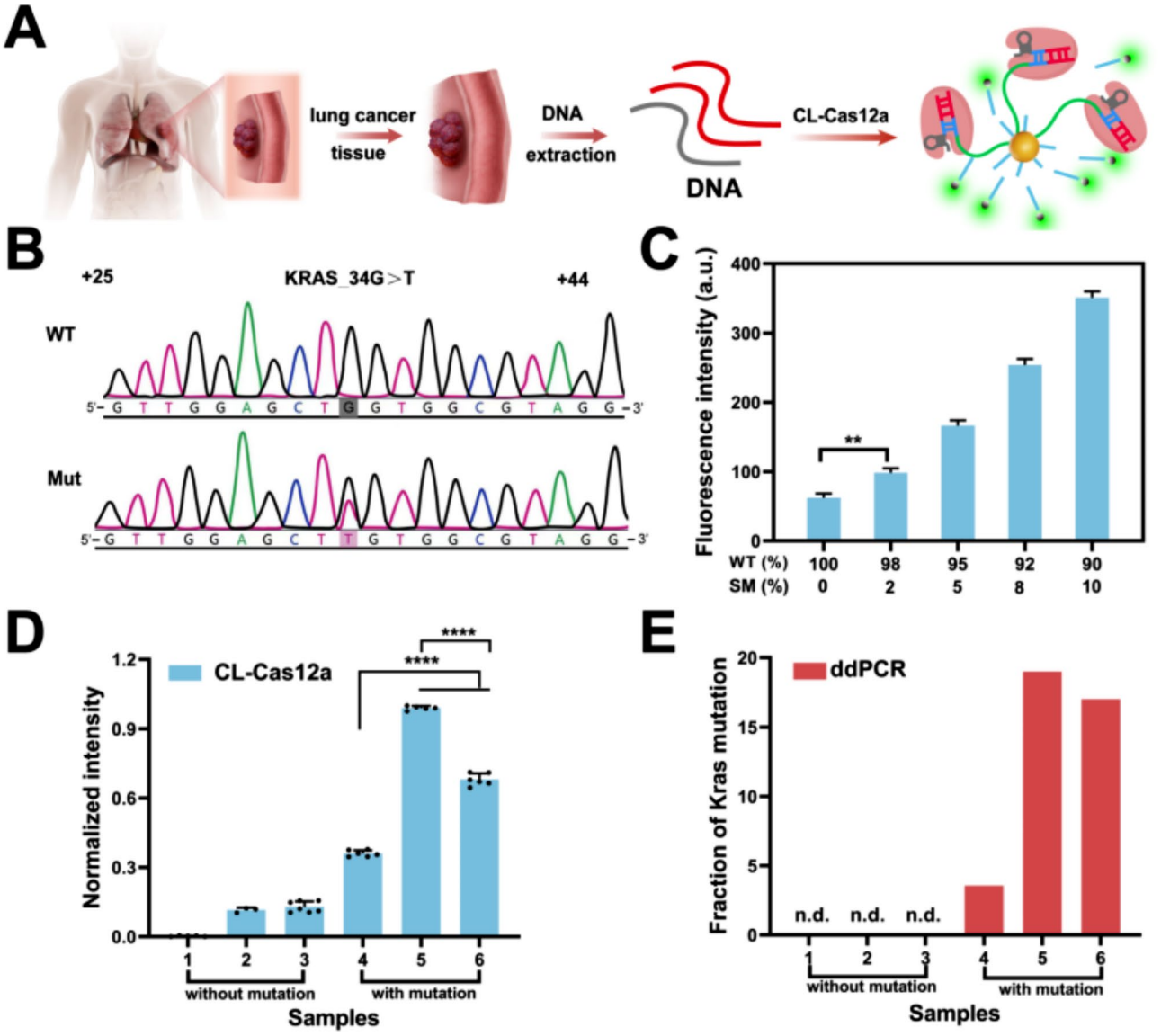

Fig. 5 Analysis of CL-Cas12a in cancer-associated SM diagnosis. (**A**) Schematic illustration for the detection of lung cancer–associated SM in human tissue samples by CL-Cas12a. (**B**) Verification of KRAS_34G > T in the genome of lung cancer tissue by DNA sequencing. The positive strand of KRAS from + 25 to + 44 is shown. (**C**) Fluorescence signals of DNA with different mutation rates. The total amount of DNA in each sample is 50 nM. (**D**) Fluorescence signals of the DNA from different tissue samples in CL-Cas12a. Lung tissue samples without KRAS mutations (1 to 3) and three patients with KRAS_34G > T mutations (4 to 6) were tested, respectively. Data represent means ± SD. *****P* < 0.0001, Student's t test. (**E**) Fraction of Kras mutation of six samples by ddPCR

been previously established using computed tomography (Fig. 5B and Figure S13; Table S4). To confirm the ability of the CL-Cas12a system to identify patients with a small fraction of mutated tumor, we mixed samples with different concentration ratios (0 to 10%) of mutation DNA to WT DNA. The results revealed that CL-Cas12a enabled distinguishing the mutation of KRAS_34G > T at a low rate of 2% (Fig. 5C). The signals from lung cancer tissues carrying the KRAS_34G > T mutation were 2.1- to 24.3-fold greater than from nonmutated samples (Fig. 5D). This differentiation cannot be achieved with the L-Cas12a system (Figure S14). The results obtained by CL-Cas12a were comparable to droplet digital PCR (Fig. 5E). Thus, the high specificity of this platform can be leveraged for clinical diagnostics of cancer-related single-base mutations.

Versatile CL-Cas12a platform for mRNA imaging in living cells

To demonstrate the versatility of CL-Cas12a, which traditionally recognizes target DNA, we designed blocked crRNA sequences that enable the CL-Cas12a to detect RNA. Survivin mRNA was chosen due to its important function in tumor diagnosis [42] and progression

monitoring [43]. The crRNA was blocked by the hairpin design, which can be unfolded by target mRNA via toehold-mediated strand displacement. The substrate switches the CRISPR/Cas12a system from "OFF" to "ON," causing digestion of the hairpin reporter and recovery of FAM fluorescence (Fig. 6A).

Before imaging in living cells, we tested the feasibility of the system in vitro. Only when all components were added would there be a significant fluorescent signal (Figure S15). Additionally, the number of base pairs in the stem of crRNA was optimized with 14 bp (Figure S16). Compared with normal A549 cells, confocal laser-scanning microscopy showed that mRNA mimic-treated A549 cells (b) demonstrated stronger fluorescence. In contrast, no fluorescence was observed in mRNA inhibitor-treated cells (c), confirming the feasibility of CL-Cas12a for targeted mRNA imaging in living cells (Fig. 6B).

Moreover, CL-Cas12a (a) yielded a significantly stronger signal than L-Cas12a (d), demonstrating its superior signal amplification. CL-Cas12a detection of mRNA in A549 (a), H292 (e), and 16HBE (f) cells showed a range of signal strengths, H292 > A549 > 16HBE (Fig. 6B), consistent with prior data and qRT-PCR results (Figure S17) [44]. Normalized intensities are shown in Fig. 6C. The good stability was confirmed by detecting the

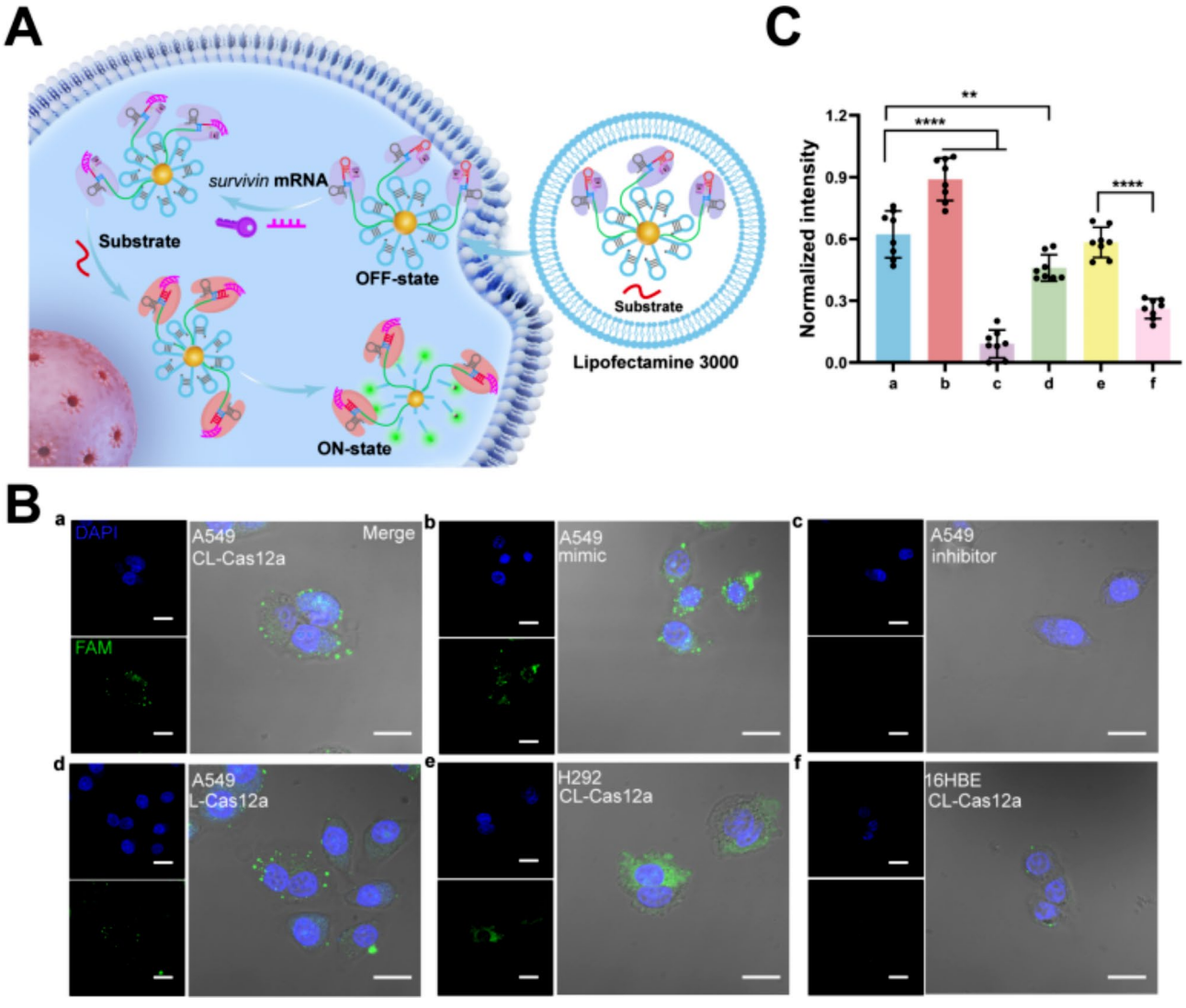

Fig. 6 *Survivin* mRNA visualization in living cells by CL-Cas12a. (**A**) Schematic illustration of the CL-Cas12a system for intracellular *Survivin* mRNA imaging. (**B**) Confocal laser scanning microscopy (CLSM) imaging of cellular *Survivin* mRNA in (**a**) A549 cells with the CL-Ca12a system, (**b**) *Survivin* mRNA mimic-pretreated A549 cells with the CL-Ca12a system, (**c**) *Survivin* mRNA inhibitor-pretreated A549 cells with the CL-Ca12a system, (**d**) A549 cells with L-Cas12a system (**e**) H292 cells with the CL-Ca12a system, and (**f**) 16HBE cells with the CL-Ca12a system. Scale bar: 20 μm. (**C**) Fluorescence signals obtained from above confocal cell samples. Data were represented as mean ± SD ($n = 8$ samples per group). Statistical significance was calculated by one-way ANOVA with Tukey's post hoc test. (* $p < 0.05$; ** $p < 0.01$; *** $p < 0.001$; **** $p < 0.0001$)

fluorescence intensity within the cells for 8 h (Figure S18).

Conclusion

Here, we present a simple and sensitive biosensor for high-sensitivity nucleic acid detection based CL-Cas12a. The CL-Cas12a system was synthesized within 15 min with high load efficiency by concentrating the substrates in the voids between ice microcrystal, thus achieving high sensitivity and efficiency. Based the CL-Cas12a, this biosensor demonstrated a broad linear range from 100 aM to 1pM with a LOD of 98 aM. The outstanding sensitivity, stability and reproducibility of proposed biosensor demonstrate some unique features including easy to prepare, rapid, and low-cost. Moreover, this CL-Cas12a based platform was successful applied for DNA testing and single-base mutation analysis, as well as intracellular *survivin* mRNA imaging. The CL-Cas12a system also serves as a versatile and programmable platform that can be configured with specific crRNA sequences to detect different targets. This study demonstrated a CL-Cas12a synthesized by co-freezing method and applied it to detect and image nucleic acids sensitively and rapidly for the first time, which provides a promising new approach to disease diagnosis and treatment monitoring.

Experimental section

Materials

All DNA and RNA oligonucleotides were synthesized by BGI Gene Technology Co., Ltd (Beijing, China). The base sequences can be found in Supplementary information (Table S2). LbCas12a and NEBuffer 2.1 were purchased from NEB (New England BioLabs, Guangzhou, China). Tris(2-carboxyethyl) phosphine (TCEP) was obtained from Sigma. The 20 bp DNA Marker, 6 × Loading Buffer, and 4 S Red Plus Nucleic Acid Stain were procured from Takara (Dalian, China). Chloroauric acid hydrate ($HAuCl_4{\cdot}3H_2O$, 99%) was acquired from Shanghai Aladdin Biotechnology Co., Ltd. The DNA extraction kit was purchased from Ikeri (Guangzhou, China) and the Trizol reagent was provided by Fdbio Science (Hangzhou, China). The TNaK buffer was composed of 20 mM Tris-HCl, 125 mM NaCl, and 20 mM KCl. Lipofectamine 3000 was obtained from HyClone (Logan, UT, USA).

Synthesis of AuNPs

We prepared 25 nm gold nanoparticles (AuNPs) using a method from the literature [26]. Briefly, all glassware was firstly cleansed by soaking in aqua regia (HNO3:HCl=1:3) for at least 30 min, then thoroughly rinsed with ultrapure water. Following that, 100 mL of a 1 mM $HAuCl_4$ solution was placed into a 250 mL flask and brought to a boil. Then 6 mL of a 38.8 mM sodium citrate solution was rapidly added, all the while maintaining stirring. This process led to the solution transition from a pale yellow to a wine-red color within 20 min. After the color change, heating was ceased, and the solution was allowed to cool to room temperature. The sizes of the nanoparticles were verified using TEM analysis. Finally, the synthesized AuNP solutions were stored at 4 °C in darkness for future use.

Characterization of AuNPs

AuNPs were diluted with nuclease-free water to a concentration of 1 nM. The AuNPs particles are then dispersed using sonication to ensure that they are as uniformly distributed as possible before detection with the instruments. The DLS and Zeta potential measurements are performed using the Malvern Zetasizer Nano ZS90 from the UK, TEM measurements are carried out with the Hitachi HT7800, and UV-vis analyses are conducted using the Varioskan LUX micrometer.

Preparation of the CL-Cas12 system

We utilized the freeze-thaw method to immobilize the FAM-labeled thiolated reporter onto the AuNPs surface. In brief, the thiolated DNA strands including hairpin reporter and linker ssDNA were first mixed with TCEP in the appropriate ratio and reduced at room temperature for 30 min. Then mix the thiolated DNA strands with AuNPs and the crRNA/Cas12a complex, and place in a freezer for 15 min. After thawing, the product was centrifuged three times (10000 g, 30 min, 4 °C) and resuspended in deionized water to eliminate any unbound DNA, crRNA/Cas12a complex and wash the AuNPs.

In this CL-Cas12a system, the hairpin reporter and linker ssDNA are anchored to the 25 nm AuNPs via Au-S bonding. The FAM-modified 3' end of the hairpin reporters are in close proximity to the AuNPs, effectively quenching FAM through FRET. Linker ssDNA facilitates the attachment of the Cas12a/crRNA complex, enabling close proximity between Cas12a and the reporter for target detection. Upon the presence of the target, Cas12a is activated, cutting the reporters along the AuNPs surface, and releasing FAM, leading to a fluorescence signal.

Modification of AuNPs using salt-aging method

AuNPs (200 μL,50 nM) solution was mixed with hairpin reporter (80 μL,10 μM) and linker ssDNA (20 uL,10 μM) and incubated for 24 h. Utilize 2 M NaCl, 0.01 M PBS to gradually increase the NaCl concentration to 0.05 M, while maintaining the SDS concentration at 0.01%. This process is repeated after increasing the NaCl concentration by an additional 0.05 M, and subsequently for every 0.1 M increase in NaCl, until the NaCl concentration reaches 1.0 M. Following the salting process, proceed with incubation overnight at room temperature. After incubating for 24 h, the particles were washed three

times with 0.01 M phosphate buffer (0.1 M NaCl, pH 7.4) through centrifugation (10000 g) at 4 °C for 30 min to remove excess DNA strands and the resulted conjugates were resuspended in deionized water. Finally, add Cas12a/crRNA complex to the mixture and incubate at 37 °C for 1 h, then centrifuge to remove unbound Cas12a/crRNA complex.

Fluorometric quantification of DNA density on AuNPs

To measure the number of DNA strands on AuNPs, 5'-thiolated DNA, with an extra fluorescent marker (FAM or Cy5) at the terminus (3') was used to prepare SNAs. A complementary sequence containing a Cy5 tag is being introduced into the system to quantify the number of linker ssDNA. Hairpin reporter: linker ssDNA mixing molar ratios were fixed at 3:1. The resulting SNAs were incubated with TCEP at 60℃ for 5 h to displace fluorescent DNA from the AuNPs. Quantification of the detached DNA utilized a standard addition method to mitigate matrix effects on the measured fluorescence intensities. Fluorescence excitation occurred at 495 nm, and emission was recorded from 500 to 600 nm. Three separate batches of prepared SNAs were employed to determine an average DNA grafting density.

The trans-cleavage ability of LbCas12a on hairpin DNA

Hairpin (1 μM, 2 μL), HPV16 (1 μM, 2 μL), and Cas12a/crRNA (500 nM, 5 μL) were used to verify the digestion of hairpins by Cas12a. 12% polyacrylamide gel electrophoresis (PAGE) was performed, with different samples mixed with 6× loading buffer (Takara, Dalian, China) and injected into the gel lanes in 0.5×Tris-acetate-EDTA (TAE) buffer. The PAGE ran at 150 V for 50 min. After electrophoresis, the gel was stained with 4 S Green Plus, and imaged using a Chemiluminescence Imaging System purchased from Guangyi Biotechnology Co., Ltd (Guangzhou, China).

Fluorescence measurement

The total reaction system consisted of crRNA/Cas12a (50 nM, 6 μL), target (1 μM, 6 μL), hairpin reporter (1 μM, 6 μL), linker ssDNA (1 μM, 2 μL), 25 nm AuNP (30 μL, 50 nM) and 6 μL NEBuffer 2.1(10×). The fluorescence signal was recorded using luminescence spectrometer (PerkinElmer LS-55, USA) with an excitation wavelength and 488 nm and emission wavelength of 515 nm).

Real-time fluorescence monitoring test

LbCas12a (50 nM) and its corresponding crRNA were combined in 10 × NEBbuffer 2.1 at a final ratio of 1:1 and mixed with CL-Cas12a system. Subsequently, real-time fluorescence scanning was initiated immediately upon addition of the target.

Evaluate the trans-cleavage activity of Cas12a on different systems

To initiate the experimental procedures, three different systems were prepared: the L-Cas12a system, the SL- Cas12a system, and the CL-Cas12a system. For the assessment of the trans-cleavage activity of Cas12a on these systems, we mixed Cas12a and crRNA in a 1:1 ratio within a 10 × NEBuffer 2.1 solution. Subsequently, equal amounts of reporters were individually placed into 1.5 mL centrifuge tubes. To each tube containing the reporter probe, 6 μL of the target (1 μM) was added, followed by the addition of 12 μL of the Cas12a/CrRNA complex (50 nM). The mixture was then incubated at 37 °C for 30 min, allowing for the necessary reactions to take place. During this incubation period, we recorded the fluorescence change ($F - F_0$), where F represents the fluorescence value after adding the target, and F_0 represents the fluorescence value without adding the target.

Cell culture and preparation

CaSki cells (human cervical cancer cells), HeLa cells (human cervical adenocarcinoma cells), A549 cells (human alveolar basal epithelial cells in lung cancer), and H292 cells (human mucoepidermoid pulmonary carcinoma cells) were used as the positive cells, whereas 16HBE cells (human bronchial epithelial cell line) were used as negative cells, and all were purchased from the Wuhan Pricella Biotechnology Co., Ltd. (Wuhan, China). Cells were cultured in Dulbecco's Modified Eagle Medium (DMEM) Medium supplemented with 10% fetal bovine serum. All of them were incubated with a 1% penicillin–streptomycin–gentamicin mixed solution at 37 °C and 5% CO_2.

The qRT-PCR analysis

To extract the human DNA from CaSki, HeLa, and 16HBE cells, the DNA Kit was used following the manufacturer's instructions. The concentration of the extracted DNAs was routinely measured using the NanoDrop spectrophotometer (Thermo Fisher Scientific, China). For the quantitative real-time polymerase chain reaction (qRT-PCR) experiment, a BlazeTaq™ SYBR Green qPCR Mix 2.0 kit was employed. Finally, three types of cells were combined with an equal amount of DNA for CL-Cas12a detection.

Detection of Swab samples using CL-Cas12a

The healthy human swab samples used in this study were provided by the Southern Medical University Nanfang Hospital. We used Huayin Biological DNA Extraction Kits purchased from Guangdong Huayin Medical Science and Technology Co., Ltd. (Guangzhou, China) to extract DNA from the swabs. Subsequently, the extracted DNA,

which included the target of interest, was subjected to detection using the CL-Cas12a system.

Detection of tissue samples from lung cancer

The DNA from six lung tissue samples was detected with CL-Cas12a and L-Cas12a system. In addition, the Sanger sequencing and ddPCR dates were provided by Yongnuo Medical Laboratory Co.Ltd. (Guangzhou, China).

Data standardization

To standardize the comparison standard among the fluorescence signals of wild-type (WT) target and SM strands, patient samples in CL-Cas12a and qRT-PCR, DNA from lung tissue, and confocal cell samples, the original variables need to be unified before analyzing the data. The original data is transformed according to a certain ratio to ensure it ranges between 0 and 1. Employing the range standardization method, each data is calculated using the following formula: $X' = (X - Xmin)/(Xmax - Xmin)$, resulting in the normalized signal.

The qRT-PCR analysis of *Survivin* mRNA in different cells

Total RNAs were extracted from A549, H292, and 16HBE cells using the Trizol Reagent Kit. To assess the expression of *Survivin* mRNA, complementary DNA (cDNA) samples were synthesized using the SureScript™ First-Strand cDNA Synthesis Kit. Subsequently, RT quantitative PCR (qPCR) analysis was conducted using the BlazeTaq™ SYBR Green qPCR Mix 2.0 kit. The primer sequences utilized in these experiments are provided in Table S2. The procedure involved the following steps: a 20 μL reaction mixture was incubated at 50 ℃ for 30 min, followed by a denaturation step at 95 ℃ for 2 min. Subsequently, 45 cycles were performed consisting of denaturation at 95 ℃ for 15 s and annealing/extension at 60 ℃ for 30 s. β-actin RNA was used as an internal control for normalization. The $2^{-(\Delta\Delta Ct)}$ method was employed to calculate the relative expression level of *Survivin* mRNA.

Transfection of CL-Cas12a system and confocal fluorescence imaging

All cells were seeded onto confocal culture dishes and incubated for 24 h. Subsequently, the CL-Cas12a or L-Cas12a system, and the substrate were mixed with 8 μL Lipofectamine 3000 for 10 min. Then the above solutions were added into the seeded cells and incubated continuously for 4 h. The change of *Survivin* mRNA concentration in living cells was achieved by transfecting *Survivin* mRNA mimic strands or *Survivin* mRNA inhibitor strands into cells for 2 h before use. The transfection process was carried out at 37 °C in a 5% CO_2 environment. After transfection, the cells were washed three times with PBS. Then, 50 μL of 4′,6-diamidino-2-phenylindole (DAPI) solution (5 g/mL) was added to the washed cells and incubated for 15 min. Following the DAPI staining, the cells were fixed with formalin for 15 min. Confocal fluorescence imaging was performed using an Olympus FV3000 confocal microscope. All images were acquired using a 100 × oil immersion objective and were subsequently analyzed using ImageJ software.

Supplementary Information

The online version contains supplementary material available at https://doi.org/10.1186/s12951-024-02831-8.

Supplementary Material 1

Acknowledgements

This study was supported by the National Natural Science Foundation of China (82072382, 82272424), the Guang Dong Basic and Applied Basic Research Foundation of China (2023A1515011195, 2023A1515010909), the Guang Dong Natural Science Foundation of China (2023A1515012629), the Guangxi Natural Science Foundation (2022JJB140002), and the high level talent project of the Affiliated Hospital of Youjiang Medical University for Nationalities (R202210302).

Author contributions

Lifeng Zhang: Experimentation, Writing. Shihua Luo: Conceptualization, Writing. Wenbin Li: Experimentation. Wanting Su: Experimentation. Siting Chen: Experimentation. Chunchen Liu: Experimentation. Weilun Pan: Experimentation. Bo Situ: Experimentation, Writing, Editing. Ling li: Conceptualization, Writing, Editing. Lei Zheng: Conceptualization, Writing, Editing. Xiaohui Yan: Conceptualization, Writing, Editing. Ye Zhang: Conceptualization, Writing, Experimentation.

Data availability

No datasets were generated or analysed during the current study.

Declarations

Ethics statement and consent to participate

All clinical samples used in this study were collected from Nanfang Hospital, Southern Medical University according to the institutional ethical guideline laid down in 1964 Declaration of Helsinki. The study was approved by the regional ethics committee (NFEC-2022-220).

Competing interests

The authors declare no competing interests.

Author details

[1]Department of Laboratory Medicine, Guangdong Provincial Key Laboratory of Precision Medical Diagnostics, Guangdong Provincial Key Laboratory of Single Cell Technology and Application, Nanfang Hospital, Southern Medical University, Guangzhou 510515, P.R. China
[2]Guangdong Engineering and Technology Research Center for Rapid Diagnostic Biosensors, Nanfang Hospital, Southern Medical University, Guangzhou 510515, China
[3]Center for Clinical Laboratory Diagnosis and Research, Affiliated Hospital of Youjiang Medical University for Nationalities, Baise, Guangxi 533000, China
[4]School of Medical Technology, Guangdong Medical University, Dongguan 523808, China
[5]Key Laboratory of Research on Clinical Molecular Diagnosis for High Incidence Diseases in Western Guangxi of Guangxi Higher Education Institutions, Affiliated Hospital of Youjiang Medical University for Nationalities, Baise, Guangxi 533000, China
[6]School of Basic Medical Sciences, Southern Medical University, Guangzhou 510515, P.R. China
[7]Medical Research Center of Nanfang Hospital, Southern Medical University, Guangzhou 510515, P.R. China

Received: 13 December 2023 / Accepted: 2 September 2024
Published online: 05 October 2024

References

1. Wang B, Wang R, Wang D, Wu J, Li J, Wang J, Liu H, Wang Y. Cas12aVDet: a CRISPR/Cas12a-Based platform for Rapid and Visual Nucleic Acid Detection. Anal Chem. 2019;91:12156–61.
2. Tang L, Wang Y, Li Y, Feng H, Lu J, Li J. Preparation, structure, and Electrochemical Properties of Reduced Graphene Sheet Films. Adv Funct Mater. 2009;19:2782–9.
3. Schlucker S. Surface-enhanced Raman spectroscopy: concepts and chemical applications. Angew Chem Int Ed Engl. 2014;53:4756–95.
4. Cui Y, Chen F, Yin XB. A ratiometric fluorescence platform based on boric-acid-functional Eu-MOF for sensitive detection of H(2)O(2) and glucose. Biosens Bioelectron. 2019;135:208–15.
5. Kosuke Sugawa TT, Tahara H, Yamaguchi D, Akiyama T, Otsuki J, Kusaka Y. Nobuko Fukuda, and Hirobumi Ushijima: metal-enhanced fluorescence platforms based on Plasmonic ordered copper arrays: Wavelength Dependence of Quenching and Enhancement effects. ACS Nano. 2013;7:9997–10010.
6. Ye Z, He W, Zhang Z, Qiu Z, Zhao Z, Tang BZ. AIEgens for microorganism-related visualization and therapy. Interdisciplinary Med. 2023;1:e20220011.
7. Wang H, Zhao E, Lam JWY, Tang BZ. AIE luminogens: emission brightened by aggregation. Mater Today. 2015;18:365–77.
8. Yao C, Zhang R, Tang J, Yang D. Rolling circle amplification (RCA)-based DNA hydrogel. Nat Protoc. 2021;16:5460–83.
9. Zhao Y, Chen F, Li Q, Wang L, Fan C. Isothermal amplification of nucleic acids. Chem Rev. 2015;115:12491–545.
10. Jeon Y, Choi YH, Jang Y, Yu J, Goo J, Lee G, Jeong YK, Lee SH, Kim IS, Kim JS, et al. Direct observation of DNA target searching and cleavage by CRISPR-Cas12a. Nat Commun. 2018;9:2777.
11. Gootenberg JS, Abudayyeh OO, Kellner MJ, Joung J, Collins JJ, Zhang F. Multiplexed and portable nucleic acid detection platform with Cas13, Cas12a, and Csm6. Science. 2018;360:439–44.
12. Kellner MJ, Koob JG, Gootenberg JS, Abudayyeh OO, Zhang F. SHERLOCK: nucleic acid detection with CRISPR nucleases. Nat Protoc. 2019;14:2986–3012.
13. Li Z, Zhao W, Ma S, Li Z, Yao Y, Fei T. A chemical-enhanced system for CRISPR-Based nucleic acid detection. Biosens Bioelectron. 2021;192:113493.
14. Mujahed I, Mustafa a, Makhawia AM. SHERLOCK and DETECTR: CRISPR-Cas systems as potential Rapid Diagnostic tools for Emerging Infectious diseases. J Clin Microbiol. 2021;59:10–1128.
15. Nguyen LT, Smith BM, Jain PK. Enhancement of trans-cleavage activity of Cas12a with engineered crRNA enables amplified nucleic acid detection. Nat Commun. 2020;11:4906.
16. Pena JM, Manning BJ, Li X, Fiore ES, Carlson L, Shytle K, Nguyen PP, Azmi I, Larsen A, Wilson MK, et al. Real-Time, multiplexed SHERLOCK for in Vitro Diagnostics. J Mol Diagn. 2023;25:428–37.
17. Luo S, Wu Y, Pan W, Zhong G, Situ B, Li B, et al. An integrated magneto-fluorescent nanosensor for rapid and sensitive detection of tumor-derived exosomes. Sens Actuators B Chem. 2023;374:132792. https://doi.org/10.1016/j.snb.2022.132792
18. van Dongen JE, Berendsen JTW, Steenbergen RDM, Wolthuis RMF, Eijkel JCT, Segerink LI. Point-of-care CRISPR/Cas nucleic acid detection: recent advances, challenges and opportunities. Biosens Bioelectron. 2020;166:112445.
19. Zahra A, Shahid A, Shamim A, Khan SH, Arshad MI. The SHERLOCK platform: an insight into advances in viral Disease diagnosis. Mol Biotechnol. 2023;65:699–714.
20. Li F, Li J, Yang W, Yang S, Chen C, Du L, Mei J, Tang Q, Chen X, Yao C et al. Framework-Hotspot enhanced trans cleavage of CRISPR-Cas12a for clinical samples detection. Angew Chem Int Ed 2023, 62.
21. Luo T, Li J, He Y, Liu H, Deng Z, Long X, Wan Q, Ding J, Gong Z, Yang Y, Zhong S. Designing a CRISPR/Cas12a- and Au-Nanobeacon-based diagnostic Biosensor Enabling Direct, Rapid, and sensitive miRNA detection. Anal Chem. 2022;94:6566–73.
22. Pei H, Li F, Wan Y, Wei M, Liu H, Su Y, Chen N, Huang Q, Fan C. Designed Diblock Oligonucleotide for the synthesis of spatially isolated and highly hybridizable functionalization of DNA-Gold nanoparticle nanoconjugates. J Am Chem Soc. 2012;134:11876.
23. Hao Y, Li Y, Song L, Deng Z. Flash synthesis of spherical nucleic acids with record DNA density. J Am Chem Soc. 2021;143:3065–9.
24. Huang M, Xiong E, Wang Y, Hu M, Yue H, Tian T, Zhu D, Liu H, Zhou X. Fast microwave heating-based one-step synthesis of DNA and RNA modified gold nanoparticles. Nat Commun 2022, 13.
25. Hu M, Yuan C, Tian T, Wang X, Sun J, Xiong E, Zhou X. Single-Step, Salt-Aging-Free, and thiol-free freezing construction of AuNP-Based bioprobes for advancing CRISPR-Based Diagnostics. J Am Chem Soc. 2020;142:7506–13.
26. Zhang X, Servos MR, Liu J. Instantaneous and quantitative functionalization of gold nanoparticles with thiolated DNA using a pH-assisted and surfactant-free route. J Am Chem Soc. 2012;134:7266–9.
27. Ye Y, Hao Y, Ye M, Song X, Deng Z. Evaporative drying: a General and readily scalable Route to spherical nucleic acids with quantitative, fully tunable, and record-high DNA loading. Small. 2022;18:e2202458.
28. Yun Zhu XX, Mengyao Cao L, Li C. Fan, Hao Pe: accelerating DNA computing via freeze-thaw cycling. Sci Adv 2023.
29. Liu B, Liu J. Freezing Directed Construction of Bio/Nano Interfaces: Reagentless Conjugation, denser spherical nucleic acids, and Better Nanoflares. J Am Chem Soc. 2017;139:9471–4.
30. Xiao Y, Liu W, Zhang Y, Zheng S, Liao J, Shan H, Tian B, Wu T, Zhang L, Tu Z et al. Simple and rapid co-freezing construction of SERS signal probes for the sensitive detection of pathogens. Chem Eng J 2023, 466.
31. Castellsague X, Alemany L, Quer M, Halec G, Quiros B, Tous S, Clavero O, Alos L, Biegner T, Szafarowski T, et al. HPV involvement in Head and Neck cancers: Comprehensive Assessment of biomarkers in 3680 patients. J Natl Cancer Inst. 2016;108:djv403.
32. Meissner JD. Nucleotide sequences and further characterization of human papillomavirus DNA present in. J Gen Virol 1999.
33. Wang X, Lou X, Wang Y, Guo Q, Fang Z, Zhong X, Mao H, Jin Q, Wu L, Zhao H. QDs-DNA nanosensor for the detection of hepatitis B virus DNA and the single-base mutants. Biosens Bioelectron. 2010;25:1934–40.
34. Pang Y, Li Q, Wang C, zhen S, Sun Z, Xiao R. CRISPR-cas12a mediated SERS lateral flow assay for amplification-free detection of double-stranded DNA and single-base mutation. Chem Eng J 2022, 429.
35. Kou Q, Wang L, Zhang L, Ma L, Fu S, Su X. Simulation-assisted localized DNA logical circuits for Cancer biomarkers detection and imaging. Small. 2022;18:e2205191.
36. Hart JR, Zhang Y, Liao L, Ueno L, Du L, Jonkers M, Yates JR 3rd, Vogt PK. The butterfly effect in cancer: a single base mutation can remodel the cell. Proc Natl Acad Sci U S A. 2015;112:1131–6.
37. Denis JA, Patroni A, Guillerm E, Pepin D, Benali-Furet N, Wechsler J, Manceau G, Bernard M, Coulet F, Larsen AK, et al. Droplet digital PCR of circulating tumor cells from colorectal cancer patients can predict KRAS mutations before surgery. Mol Oncol. 2016;10:1221–31.
38. Choi HJ, Moon JH, Kim HK, Lee YN, Lee TH, Cha SW, Cho YD, Park SH. KRAS mutation analysis by next-generation sequencing in endoscopic ultrasound-guided sampling for solid liver masses. J Gastroenterol Hepatol. 2017;32:154–62.
39. Altimari A, de Biase D, De Maglio G, Gruppioni E, Capizzi E, Degiovanni A, D'Errico A, Pession A, Pizzolitto S, Fiorentino M, Tallini G. 454 next generation-sequencing outperforms allele-specific PCR, Sanger sequencing, and pyrosequencing for routine KRAS mutation analysis of formalin-fixed, paraffin-embedded samples. Onco Targets Ther. 2013;6:1057–64.
40. Pao W, Wang TY, Riely GJ, Miller VA, Pan Q, Ladanyi M, Zakowski MF, Heelan RT, Kris MG, Varmus HE. KRAS mutations and primary resistance of lung adenocarcinomas to gefitinib or erlotinib. PLoS Med. 2005;2:e17.
41. Canon J, Rex K, Saiki AY, Mohr C, Cooke K, Bagal D, Gaida K, Holt T, Knutson CG, Koppada N, et al. The clinical KRAS(G12C) inhibitor AMG 510 drives anti-tumour immunity. Nature. 2019;575:217–23.
42. Liu YH, Gao JL, Liu JX, Liu D, Fang WK, Zheng B, Tang HW, Li CY. Photo-gated and self-powered three-dimensional DNA motors with boosted biostability for exceptionally precise and efficient tracing of intracellular *survivin* mRNA. Biosens Bioelectron. 2021;190:113445.
43. Stobiecka M, Ratajczak K, Jakiela S. Toward early cancer detection: focus on biosensing systems and biosensors for an anti-apoptotic protein *survivin* and *survivin* mRNA. Biosens Bioelectron. 2019;137:58–71.
44. Schiffman M, Doorbar J, Wentzensen N, de Sanjose S, Fakhry C, Monk BJ, Stanley MA, Franceschi S. Carcinogenic human papillomavirus infection. Nat Rev Dis Primers. 2016;2:16086.

Publisher's note